Williamsburg, Virginia
ACTIVE 04
2004 September 20-22

The Impact of Model Uncertainty on Spatial Compensation in Active Structural Acoustic Control

Joseph D. Sprofera
Duke University
Pratt School of Engineering
Durham, NC 27708
jds27@duke.edu

Robert L. Clark
Duke University
Pratt School of Engineering
Durham, NC 27708
rclark@duke.edu

Randolph H. Cabell
Structural Acoustics Branch
NASA Langley Research Center
Hampton VA 23681
r.h.cabell@larc.nasa.gov

Gary P. Gibbs
Quiet Aircraft Technology Project
NASA Langley Research Center
Hampton VA 23681
g.p.gibbs@larc.nasa.gov

Abstract

Turbulent boundary layer (TBL) noise is considered a primary factor in the interior noise experienced by passengers aboard commercial airliners. There have been numerous investigations of interior noise control devoted to aircraft panels; however, practical realization is a challenge since the physical boundary conditions are uncertain at best. In most prior studies, pinned or clamped boundary conditions have been assumed; however, realistic panels likely display a range of varying boundary conditions between these two limits. Uncertainty in boundary conditions is a challenge for control system designers, both in terms of the compensator implemented and the location of actuators and sensors required to achieve the desired control. The impact of model uncertainties, uncertain boundary conditions in particular, on the selection of actuator and sensor locations for structural acoustic control are considered herein. Results from this research effort indicate that it is possible to optimize the design of actuator and sensor location and aperture, which minimizes the impact of boundary conditions on the desired structural acoustic control.

1. INTRODUCTION

Since the late 1980s, active control of aircraft cabin noise using smart structures has been a well-investigated research area. In many cases, passive methods of noise reduction have several key detriments, including large weight penalties (in the case of structural stiffening) and lack of broadband passive damping to deal with forced (rather than resonant) excitations. Tuned vibration absorbers were also discounted as being effective in this area due to the difficulties in maintaining the proper tuning in an environment experiencing the degree of variation exhibited by aircraft applications. Instead, an active control approach was found to be attractive due to its ability to adapt to the changing environment. Initial active control scenarios, prior to the concept of smart structures, were limited by a need to use large arrays of microphones and speakers as sensors and actuators. However, upon the introduction of smart structures into this field, the beneficial properties of the active transducers (such as low weight, high bandwidth, and spatial filtering in the case of piezos) became a selling point for active control of aircraft cabin noise.

The first investigations into using piezoceramic actuators for the active control of structurally radiate noise were initiated in 1989.[1] This work followed an earlier investigation into the active control of propeller noise by Fuller and Jones[2] and was also related to an investigation involving sound transmission from elastic plates.[3] Fuller's investigations were instrumental in shifting the focus of noise control from the passive realm (acoustic absorption methods and materials) to the active realm by attempting to control the surface of the vibrating noise source.

One major investigation into using smart structures in the active control of aircraft cabin noise was performed by Grewal, Nitzsche, Zimcik, and Leigh beginning in 1996.[4] The initial work described the preliminary investigation of using piezo patches in the attempted reduction of cabin noise for a de Havilland Dash-8 aircraft. This work, while not optimized in nature, proved that it was feasible to reduce cabin noise and fuselage vibration through the use of piezoelectric actuators. The dominant source of the disturbance for this project, however, was the propeller blade from the Dash-8.

Mathur, Tran, Simpson, and Peterson contributed to active structural acoustic control and active noise control of aircraft cabin noise in a research paper published in 1997.[5] They included broadband noise due to boundary layer turbulence as a major source of cabin noise instead of focusing on the tonal noise generated by the propeller tones.

Piezoelectric actuator locations were optimized through the use of analytical and experimental transfer function data, which led to the selection of sixteen locations to be tested. Tests showed that significant noise cancellation could be achieved at the location of a passenger's headrest; however, they determined that a practical system would still take much work to develop.

While there has been significant research into ways of countering the transmission of sound and vibration into the interior of an aircraft, the topic of variation in the boundary conditions of the panels making up the "skin" of the aircraft has not been sufficiently addressed. This can possibly be attributed to the added difficulty of optimizing a controller placement based on an additional set of variables. Now that the topic of structural acoustic control has been well investigated in regards to this application, continuing to the next step of the impact of model uncertainty, specifically in the area of boundary conditions, is a logical course of action.

There has been much research in the area of reducing the noise transmission to the interior of an aircraft cabin, but the concept of making an adaptive structure capable of handling a range of boundary conditions while still performing this function has yet to be fully explored. In past attempts at reduction of interior cabin noise, active control efforts were focused on the component resulting from acoustic and structural disturbances resulting from engine noise. However, Clark and Frampton investigated active control of turbulent boundary layer noise transmission through an aeroelastic plate in 1997.[6] This was one of several investigations by Frampton and Clark involving the study of TBL noise control and aeroelastic coupling.[7,8]

The focus of this work is the development of an adaptive structures based method of controlling the radiated sound transmitted to the interior of an aircraft while taking into account the possible variations in boundary conditions associated with the vibrating panels. The use of ideal conditions, under which the motion of the plate and its natural frequencies can both be described explicitly by mathematical equations, does not accurately reflect a real world application scenario. Real-world structures feature potentially varying boundary conditions that should be considered in any modeling approach. Determining the impact of model uncertainty, particularly the model uncertainty associated with the boundary conditions, in the realm of control is the major question to be answered in this work.

The approach taken in this project is that of a detailed mathematical model that combines structural modeling, actuator and sensor modeling, performance metrics, radiation modeling, actuator and sensor design using open-loop Hankel Singular Value (HSV) techniques, and finally the implementation of a genetics based optimization algorithm. All control in this system is attained through the use of adaptive piezoelectric sensors and actuators.[9] These sensors and actuators are modeled in state space in order to be included with the structural model in the system's state space representation.[10] The system is modeled based on energy equations, assumed functions, and an eigenvector transformation.[11]

Additionally, it is necessary to model radiation filters that are capable of taking the velocity outputs from discrete points on the structure and performing an estimate of the radiated sound power from these values. This technique has been investigated by Elliott and Johnson[12] and Gibbs et al.[13] The HSV optimization method is used to design actuator and sensor configurations that enforce the performance desires of the system while reducing the coupling to structural modes that fall beyond the bandwidth of interest. Clark and Cox[14] developed a technique that introduced this design, which was further enhanced by Smith and Clark[15] to improve its effectiveness.

Finally, a genetic algorithm, initially used by Richard and Clark[16], utilizes a modified version of the HSV scoring system to optimize a solution. By creating a completely random (limitations only on maximum patch size) pool of potential actuators or sensors, the algorithm proceeds to perform generations of patch "mating" coupled with random genetic mutations of patch characteristics. The design of spatial compensators results from the scoring of Hankel singular values (HSVs). This design metric work has been previously developed by Smith and Clark[15], Clark and Cox[14], Lim[17], Lim and Gawronski[18], and Gawronski and Lim.[19] The scoring of the HSVs is used to determine the open-loop controllability and observability Gramians and allows for a method of measuring the sensor and actuator's ability to couple to particular modes of the system as incorporated into a performance metric.

2. STRUCTURAL MODEL

A large portion of the work on this project dealt with building a mathematical model of a simply supported plate with variable rotational flexibility built into the boundary conditions. In the case of a simply supported plate, mathematical functions explicitly detail the displacement and, through differentiation, the velocity or acceleration of the plate as well. However, a simply supported plate represents an ideal that can never be achieved completely in a lab setting let alone in real-world applications. In fact, the boundary condition that many real-world applications are intended to be to would be that of the clamped end condition, which is once again not feasible. Instead, the panels investigated in this project exhibit boundary conditions between simply supported and clamped.

The overall plate system was modeled such that the plate boundaries involved a rotational stiffness, K_t, in the form of distributed rotational springs along the edges. Varying the value of these springs from zero to a very high

stiffness is potentially the same as varying the end conditions of a plate from simply supported to clamped. Both the motion of the plate and the natural frequencies will vary with the boundary conditions.

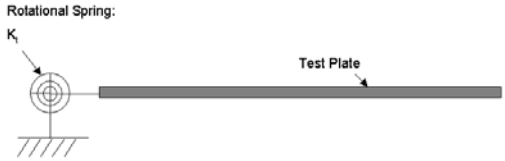

Figure 1. Depiction of rotational spring along one edge of test plate

For the structure defined by this problem, the eigenfunctions of a plate with pinned boundary conditions can be used as assumed modes since they are admissible functions.

$$\phi_{rs}(x,y) = \frac{2}{\sqrt{mab}} \sin\left(\frac{r\pi x}{a}\right) \sin\left(\frac{s\pi y}{b}\right)$$

In the above equation, ϕ_{rs} represents the normalized mode shape of the simply supported plate. Also, *m* is the density per unit area of the plate, *a* is the length of the plate in the x direction, and *b* is the length of the plate in the y direction. This function meets the requirements to be the admissible function. Therefore, this shape function will be used as the assumed function, and can be seen in the following equation:

$$w(x,y,t) = \sum_{r=1}^{M} \sum_{s=1}^{N} \phi_{rs}(x,y) \cdot \eta_{rs}(t)$$

where $\eta_{rs}(t)$ is the time domain response in modal coordinates. From this equation, the potential and kinetic energy expressions for the plate are created. The kinetic energy equation is simply the mass motion of the plate; it is not affected by the presence of the rotational springs on the edges. However, the potential energy equation includes not only the strain energy in the plate, but also the rotational energy that would be stored in the springs.[20]

$$V(t) = \frac{1}{2}\int_0^{L_x}\int_0^{L_y} D_e\left[\nabla^2 w(x,y,t)\right]^2 dy\,dx + \frac{1}{2}K_{T1}\int_0^b \left[\frac{\partial w(o,y,t)}{\partial x}\right]^2 dy$$
$$+\frac{1}{2}K_{T2}\int_0^b \left[\frac{\partial w(L_x,y,t)}{\partial x}\right]^2 dy + \frac{1}{2}K_{T3}\int_0^a \left[\frac{\partial w(x,0,t)}{\partial y}\right]^2 dx$$
$$+\frac{1}{2}K_{T4}\int_0^a \left[\frac{\partial w(x,L_y,t)}{\partial y}\right]^2 dx$$

In the above equation, D_e is $\frac{E_s h_s^{\,3}}{12(1-\upsilon_s^2)}$, where E_s is Young's modulus, h_s is the plate's thickness, and υ_s is Poisson's ratio. The K_T values represent the distributed rotational springs present along the four edges of the plate. Using the assumed modes and the kinetic and potential energy equations, it is possible to derive a mass and stiffness matrix for the system.

3. EIGENVALUES AND EIGENVECTORS

Through the use of these matrices, the eigenvalues and eigenvectors of the system can be derived. While the admissible function used is for the simply supported plate, the eigenvalues that result from this calculation are for the finite dimensional system with the rotational springs present. Therefore, springs with a value of zero will cause the eigenvalues for a simply supported plate to be returned, but springs with a very high stiffness value will cause eigenvalues close to that of a clamped plate to return.

The eigenvectors that are returned by this calculation provide ratios for building the new system as described by the rotational springs. If the springs have a value of zero, the eigenvectors will simply show that the approximate modes of the new system are composed of single natural modes of the simply supported system. The returned eigenvector will be composed of an entry for each of the modes of the system, with a one appearing in the position corresponding to the appropriate simply supported mode and zeros in all other entries. However, when there are non-zero spring values at the edges, the eigenvectors provide much more important information.

At that point, the eigenvectors explain how to build the approximate modes of the new system by combining several mode shapes from the assumed system. These eigenvectors are extremely important in determining qualities of the approximate system relative to the assumed system. If the plate is simply supported, the assumed mode can

be used to directly define the displacement, velocity, and acceleration of the plate. When the plate is not simply supported, the eigenvectors provide the means for determining these values.

$$\phi_{approximate}(j) = \Phi_{assumed} \cdot \alpha(:, j), \text{ for } j = 1 : N^2$$

In the above equation, $\Phi_{assumed}$ is a row vector of the assumed mode shapes of the system, which when evaluated at a specific point on the plate's surface will return the displacement of the various mode shapes of the plate at that point. $\phi_{approximate}(j)$ is the new mode shape of the system, found by multiplying the assumed mode shapes by the appropriate eigenvector. $\alpha(:, j)$ is the j[th] eigenvector of the modeled system, a column vector. When the rotational springs have non-zero values, the eigenvector for any approximate mode will be fully populated. The multiplication of the row vector and column vector will result in a single approximate mode shape function. Using the first eigenvector of the system will return the approximate mode shape of the first mode. Naturally, the more assumed mode shapes included in the original model, the longer the row and column vectors, and the more accurate the approximate mode shape becomes.

$$\Phi_{assumed} = \begin{bmatrix} \phi_1 & \phi_2 & \ldots & \phi_N \end{bmatrix}_{1 \times N}$$

Where,

$$\phi_i = \frac{2}{\sqrt{mab}} \sin\left(\frac{r(i)\pi x}{a}\right) \sin\left(\frac{s(i)\pi y}{b}\right), \text{ for } i = 1 : N$$

and where *N* is the number of assumed modes used in the determination of the approximate mode shapes.

Also,

$$\alpha(i, j) = \begin{bmatrix} \alpha_{11} & \alpha_{12} & . & . & . & \alpha_{1N} \\ \alpha_{21} & \alpha_{22} & & & & \\ \alpha_{31} & & . & & & \\ . & & & . & & \\ . & & & & . & \\ \alpha_{N1} & & & & & \alpha_{NN} \end{bmatrix}$$

where α is the eigenvector matrix of the approximate system.

4. RADIATION MODEL

Since the overall goal of this project is the reduction of sound transmitted through a panel, the performance by which the active structural system will be judged is radiated sound power. An attempt at measuring the radiated sound power can be made with a microphone array positioned close to the vibrating surface of the test panel inside of the anechoic test room. However, this method of collecting a measurement of radiated sound power that directly results from the plate's vibrations is too inaccurate for the purpose of this project.

Instead, the radiated sound power is estimated using a technique called Radiation Modal Expansion (RME).[12,13] This process involves collecting acceleration data from the surface of the plate and mathematically translating this information into the estimate through the use of a radiation matrix.

$$\overline{P} = a(jw)^H R(jw) a(jw)$$

In the above equation, the radiation matrix ***R*** is combined with the acceleration data taken from the plate through the use of an accelerometer array. Each accelerometer in the array represents the center of an imaginary vibrating piston. The radiation matrix correlates the phase between the centers of the pistons in a specific radiation mode. This information is then used with the acceleration measurements in determining the estimated sum of the sound radiated by the pistons.

The accuracy of the radiation estimate depends on how many data points on the surface of the plate are used and how many modes are modeled in the radiation matrix. It was found that for the purpose of this work, modeling just a single radiation mode and using fifteen accelerometers provided accuracy to within 5% of what would be predicted by modeling fifty radiation modes and using fifteen accelerometers. The far simpler use of fewer modes and the resulting quicker computation time are clearly more desirable than 5% greater accuracy in this case.

5. TRANSDUCER MODEL

The next step in the process involved the detailed modeling of the transducers present in the system. This included modeling the piezo patch pair present on the plate for control purposes. The approach taken in this research follows and was inspired by that taken in the research performed by Richard in his investigation of flutter control for a delta wing.[21] Rather than performing integration over the patch domain in each case where a new patch is defined, an element summation approach was employed.

The summation approach creates an imaginary grid of 4 mm piezo cells distributed over the entire surface of the plate. Due to the significantly small size of the cells in relation to the wavelength of the modes on the surface of the plate, it is a fair assumption to make that the displacement (or velocity or acceleration) of the individual cell is constant across its entire surface area. The electromechanical coupling and capacitance values at the center of each cell are multiplied by the cell area to get the corresponding total values. Once the boundaries of a piezo patch are defined, a close approximation of the electromechanical coupling and capacitance values of the patch can be made by summing the values for the cells found within the boundaries.

The main source of error in this approach occurs as modal wavelength decreases, since the assumption that cell values are constant across their area becomes a poor one. For the purposes of controlling radiated sound power, which is attributed to low order radiation modes, this approach remains valid. The approximation exhibits higher accuracy at the lower order modes that are targeted in radiated sound power reduction.

6. TRANSDUCER PLACEMENT SELECTION

The scoring metric used in comparing potential piezo patch pairs against each other is rooted in the calculation of the Hankel Singular Value (HSV) of a particular patch pair. The HSV of a patch pair can be physically interpreted to be a measure of the amount of energy that can be put into the system through one patch/path in relation to the amount of energy that could then be measured in the system through the other patch/path. This measure of energy input and output through the patches/paths is accomplished by examining the electromechanical coupling of the patches to the plate structure.

The actual metric that scores the piezo patch pairs includes the input/output path HSVs (input being piezo actuator, output being piezo sensor) as well as the performance/disturbance path HSVs (performance being radiated sound power and disturbance being a broadband modal disturbance) in a function that also provides for normalization. The normalization within the function as well as the use of standardized normalization values allows for easy comparison between patch pairings.

There were two additional weighting factors included in the scoring process. The first of these was the differentiation between an in-bandwidth region and an out-of-bandwidth region with regards to the frequency range of interest. The scoring metric is manipulated to reward coupling by a piezo pair to in-bandwidth radiating modes and to penalize coupling to modes found immediately out of the frequency range of interest. The frequency range of interest was identified as having an upper limit of 1000 Hz. The scoring metric, therefore, rewards patch pairs that couple well to modes whose natural frequency is below 1000 Hz. The number of modes that this describes is dependent on the current status of the boundary conditions of the system.

The modes that fall immediately beyond 1000 Hz are those that the system will attempt to de-couple to. While it would be ideal to ask the system to de-couple to any mode not in the interested bandwidth, that type of scoring parameter causes difficulty in converging on a repeatable solution under the constraints of the chosen actuator/sensor design/configuration. Asking a potential patch pair solution to couple well to simple, low order, radiating modes, and at the same time avoid coupling to modally dense, high order modes does not produce a pool of potentially viable results.

Following the scoring of a patch pair in both the in-bandwidth and out-of-bandwidth areas, the final score for the patch is assembled. The final score requires a modification to the out-of-bandwidth scores. When the out-of-bandwidth scores are initially calculated, patch pairs that couple well to the modes in the out-of-bandwidth regions will receive high score results. Instead, the final metric penalizes these patch pairs and rewards the patch pairs that couple poorly, or de-couple, to the out-of-bandwidth modes. For this reason, the inverse of the out-of-bandwidth score is taken prior to adding it with the in-bandwidth coupling score. This produces the final score by which a patch pair is graded at for a given boundary condition test.

During the optimization process, a trial patch pair is scored for each modeled boundary condition simultaneously. The overall score for an individual is then the sum of the scores from each condition. This process results in the selection of a patch pair that is optimized for the overall range of potential boundary conditions. The individual scores from each condition can be combined in a linear manner or they can be pooled in a weighted sum according to the likelihood of each of the specific modeled boundary conditions occurring.

The calculation of the HSV is accomplished using the following equation:

$$\gamma_i^2 \approx \frac{\sqrt{tr[B_i B_i^T]tr[C_i C_i^T]}}{4\zeta\omega_n}$$

This states that the HSV of a given path (*i*) is proportional to the square root of the trace of a specific path through the B and C matrix. The B matrix of the state space system represents the disturbance (w) and control (u) paths while the C matrix represents the sensor (y) and performance (z) paths. The HSV can thus be calculated for any of these paths. However, for the sake of determining the HSV scores of patch pairs, the actuator to sensor path is examined foremost, with some examination of the performance disturbance path relating to that actuator/sensor pair included. In and out-of-bandwidth scoring is accomplished using the following scoring equations:

$$J_{perf} = \sum_{i=1}^{N} \Lambda_{perf} \frac{\sigma_{yu_i}}{\overline{\sigma}_{yu_i}} \sigma_{zw_i}$$

$$J_{robust} = \sum_{i=1}^{N} \Lambda_{robust} \frac{\sigma_{yu_i}}{\overline{\sigma}_{yu_i}} \sigma_{yu_i}$$

$$\sigma_{xx_i} = \gamma_i^2$$

In these equations, the performance scoring function relates to in-bandwidth scoring while the robust scoring function relates to out-of-bandwidth scoring.

Each scoring function result is then normalized. The separate normalization of the in and out-of-bandwidth scoring results ensures that dominance of a particular patch in one of the two bandwidths does not outweigh overall performance. Additionally, the performance and robustness functions are normalized with the same values regardless of the boundary condition involved in the coupling score. This allows for comparison of scores between two separate test boundary conditions if so desired. Following normalization, the scores are combined through multiplication to create an overall score for the pair.

$$J = \bar{J}_{perf} * \bar{J}_{robust}$$

7. USE OF A GENETIC ALGORITHM

The scoring model is used in combination with a genetic algorithm approach to converge on an optimal solution for minimizing the performance function of the system.[22] There are several steps involved in the application of the genetic algorithm.

First, the algorithm requires that a patch pair, consisting of an actuator and a sensor, be treated as a single individual within the mating pool. The characteristics of each pair are reduced to a binary data string of 1s and 0s, which can be considered the DNA of the individual. Each individual has eight pieces to its DNA string that describe the height, width, x-center location, and y-center location of the actuator and sensor. Prior to converting these values to binary, they are normalized, reducing all pre-converted values into the range from 0-1.

Starting with an initial random pool of twenty individuals, the top ten individuals are selected for mating based upon their total coupling score result. Choosing the top scoring individuals for mating increases the chances of producing additional high scoring individuals. Each of the top ten individuals is mated with two other randomly selected top ten individuals. This produces twenty new offspring that are used as the next generation of individuals to be tested.

The mating process is a two-stage process, where the first stage is the actual mating of the individuals. For the mating process, once two individuals are chosen, the DNA string of each is broken as that same point and front and back ends are swapped. The use of a single random breaking point in the mating of two individuals ensures that the two offspring will each have at least seven complete characteristics of the parents and one possible characteristic that is altered due to potential breaking in the middle of an encoded parameter string. The second stage is the random genetic mutation of the new offspring. In the mutation stage, each bit within the DNA string has a set percentage change of flipping from a 1 to a 0 or vice versa. A low mutation percentage means it is not likely there will be drastic changes to the parameters that made the parents high scoring individuals, but that there is the possibility of mutation allowing for offspring to break out of local maximum scoring areas on the plate. This creates the ability for the algorithm to investigate potential patch pairs with a wide variety of parameters.

Following the mating and mutation process, the new generation of offspring is ready to be modeled and scored according to the standard scoring metric. Before returning to the scoring portion of the cycle, however, the highest scoring individual from the previous generation is inserted into the new generation. This ensures that the highest

scoring pair in each generation is at least equivalent to the highest scoring pair in the previous generation. This also provides a way of checking for convergence. Convergence of the genetic algorithm is defined as the top scoring pair remaining exactly the same for ten consecutive generations. Following the insertion of the top pair from the previous generation and the scoring of the complete individual pool, the individuals are ranked. If the top ranked pair has the exact same DNA string for ten consecutive generations, that individual is considered the optimal solution and the iteration of the mating process ceases. Typically the entire procedure would be repeated a few dozen times to produce multiple potentially optimal pairs. The power of the genetic optimization process is shown in that the overall highest scoring pairs following dozens of runs are similar.

8. PIEZOELECTRIC PATCHES

The size of a piezoelectric patch is typically limited by the fact that the ceramic material is rather brittle and forming thin patches to provide high authority/low weight actuators can lead to fractures. The industry standard for lead-zirconate titanate (PZT) patch sizes is 7.239 cm (2.85 in.). Larger patch sizes can be made, though the cost is higher, as is the likelihood of the PZT breaking during the manufacturing process.

Attempting to use a single 7.239 cm square patch as an actuator on a 0.254 m by 0.508 m (10 in. by 20 in.) plate would likely not provide the level of control that was desired. Part of the genetic optimization required establishing a maximum value for the actuator and sensor patches. The sensor patch, being made of poly-vinylidene fluoride (PVDF), could be made to match any size and shape that the genetic algorithm required. The PZT clearly required limits, though those limits needed to be above the 7.239 cm square value that the individual patches would be limited to.

To be able to replicate the size of the patch deemed necessary by the genetic algorithm, several PZT patches would need to be mounted to the plate. The PZTs would be mounted in such a way as to form the overall shape chosen by the optimization routine, and placed sufficiently close together so as to mimic the same spatial aperture on the plate. In order to determine if this attempt at recreating a larger patch from smaller pieces, it was necessary to mathematically model the two situations and compare the transfer function from actuator to sensor in each case.

The case of the large patch had already been modeled for the purpose of the genetic algorithm, making the actuator-sensor transfer function readily available. The modeling of the smaller pieces required several short but detailed steps. First, it was decided that the smaller pieces should all be of equal size. With the selected PZT size (from the genetic optimization) being 15.24 cm square (6 in. x 6 in.), and the smaller pieces needing to be 7.239 cm at the most, it was decided that the PZT pieces would be cut down to 5.08 cm (2 in.) squares and mounted in a 3 x 3 array. This would effectively reproduce a 15.24 cm square spatial window on the plate. After determining the center points of the 5.08 cm square pieces, a new electromechanical coupling model is created for the 3 x 3 patch array. The state space system corresponding to the structural system with the array of PZT patches has nine inputs and one output (the PVDF). In order to readily compare the transfer function from actuator to sensor, the nine actuator inputs must be reduced to one equivalent input. To accomplish this, a one input-nine output state space system that essentially represents distributing the same control signal to each PZT piece is created. Connecting this system with the structural system internalizes the nine actuator paths, and establishes a new structural state space system with one actuator input and one sensor output. If the gap between the PZT pieces is estimated to be sufficiently small (around 3mm or just over 0.10 in. apart, which is physically attainable during the mounting process), the difference in the transfer functions is negligible. A plot comparing the two transfer functions is shown in Figure 2. The dark line represents the modeled transfer function from actuator to sensor when the modeled actuator is a single 6-inch square PZT patch. The light line also represents a modeled transfer function, but in that case the actuator is a 3 x 3 array of 5.08 cm square PZT patches.

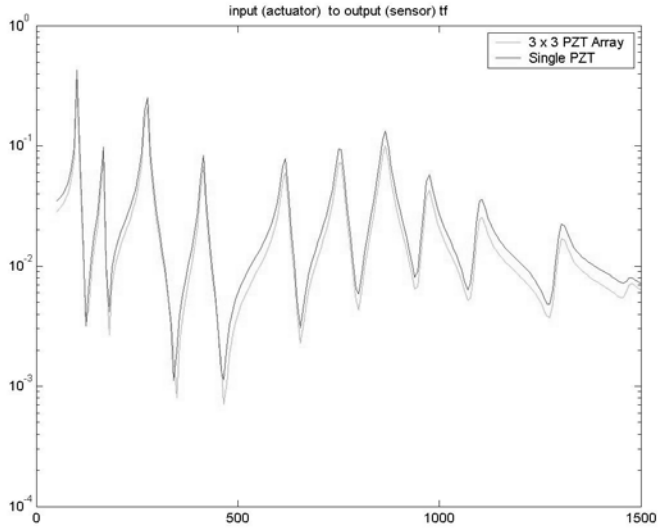

Figure 2: PZT to PVDF Transfer Function Comparison

In Figure 3, the single PZT patch is displayed in comparison with the 3 x 3 PZT array. The optimal sensor location is also shown (the darker lines).

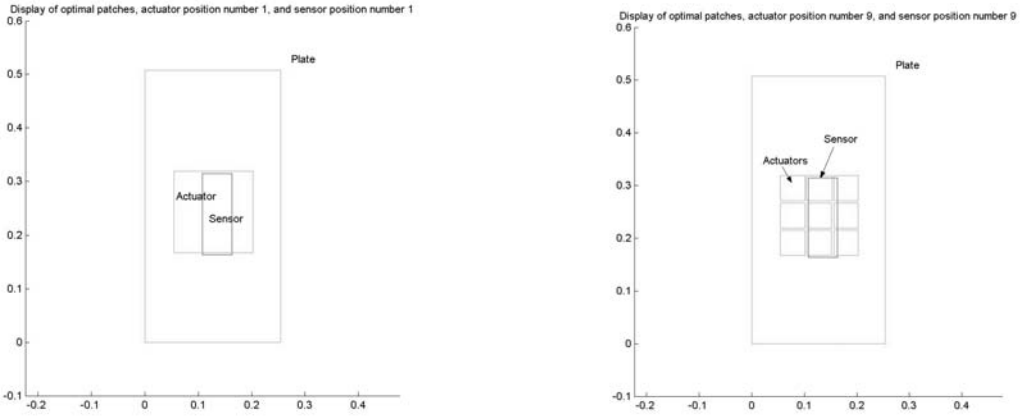

Figure 3: Full-Size PZT Patch and PZT Piece Array Comparison

9. TEST CONFIGURATION

The design of a test structure capable of mimicking multiple boundary conditions required intuitive design, pre-fabrication validation, and attention to detail. It became obvious during the course of the mathematical modeling that there would be some sacrificial design points between the theoretical and physical models. It would be impossible to perfectly replicate the mathematical model due to physical restrictions relating to the use of springs and the inability to completely model potential losses in the system. It was still important to create a physical model that came as close to possible to capturing the ideals set forth in the mathematical model and one that allowed for as dramatic as possible changes in the conditions seen at the boundaries of the test plate.

The test specimen is a 0.254 m by 0.508 m (10 in. by 20 in.), 13 gauge steel plate. An array of PZT actuators and a single PVDF patch are positioned on opposite sides of the plate according to the multi-patch diagram in Figure 3. Additionally, 15 accelerometers are located on the same side of the plate as the PVDF in a 5 x 3 evenly spaced array. The plate itself is mounted to 0.04445 m (1.75 in.) tall, thin, tempered spring steel shims. These shims prevent the plate from translating and the relative thickness of the shim dictates the rotational stiffness at the edges. The shims are mounted edge-on to the plate, held in place by 0-80 screws every 1.016 cm (0.40 in.) around the plate's perimeter. Multiple shim thicknesses were used in order to recreate several different rotational stiffness values. The shims are, in turn, connected to a large, aluminum base window-like structure that is mounted within a transmission loss test facility. The base window-like structure allows for the test plate to have an exposed surface in both the anechoic and reverberation chambers of the facility.

A large speaker producing an acoustic disturbance from a uniform random noise signal is used in the excitation of the plate. The PVDF signal is fed back to a simple LQG based controller with the purpose of minimizing the performance (radiated sound power) of the system. The accelerometer signals are conditioned using an integrated circuit piezoelectric signal conditioner while the incoming PVDF signal is converted using a charge mode amplifier to provide a voltage signal. The incoming data is collected using a data acquisition breakout box and processed with an xPC Target computer. The computer and breakout box also supply the two major outgoing input signals, the uniform random noise signal for the speaker and the control signal for the PZTs. A Simulink program built in the xPC Target environment manages the data collection.

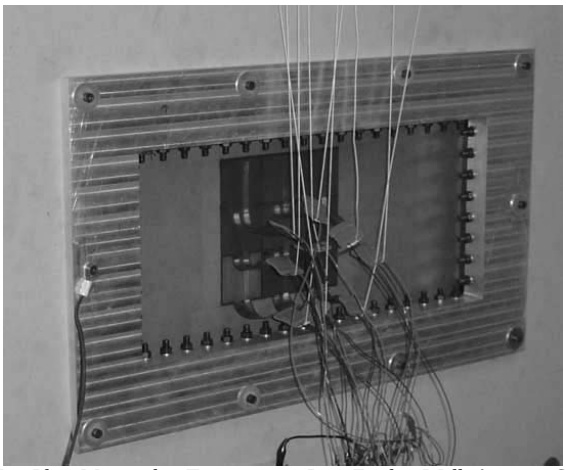

Figure 4: Test Plate Mounted in Transmission Loss Facility Wall, Actuator Side Shown

10. RESULTS

In total, eight conditions were examined, ranging from a quasi-simply supported condition that utilized 0.010 in. shims, to a condition closer to clamped, using 0.125 in. thick shims for supports. The end result of the testing demonstrated that optimizing potential actuator and sensor placements with respect to possible variations in boundary conditions has some benefit in the control of structurally radiated sound power.

			Measured Data (Shim Thickness)				
m	n	SS Pred	0.010 in.	0.062 in.	0.125 in.	Clamped Pred	% off from Clamped
1	1	103.90	103.4	149.4	148.3	206	28.01
1	3	270.13	266.7	310.3	323.9	378	14.31
2	1	353.24	360.5	413.1	416.0	536	22.39
1	4	415.58	413.2	450.6	474.5	537	11.64
2	3	519.47	503.9	565.5	585.9	700	16.30
1	5	602.59	597.7	638.1	656.3	741	11.43
2	4	664.93	647.5	705.8	729.5	849	14.08
3	1	768.82	755.9	831.7	840.1	1033	18.67
2	5	831.16	832.0	889.7	914.1	1046	12.61
3	3	935.05	905.2	981.7	1011.9	1196	15.39

Table 1: Natural Frequency Comparison, Measured vs. Predicted, All Values in Hz, Unless Noted
Predictions Founds Using Equations from Leissa's Vibration of Plates[23]

For each boundary condition tested, several actuator effort levels were examined. The actuator effort level is defined as the H_2 norm of the system whose only input is a uniform random noise disturbance and whose only output is the output of the designed controller. More aggressive controllers, created by manipulation of the signal noise floor and the controller penalty, will result in larger actuator effort level values. Matching actuator effort level values between controller tests for two different boundary conditions allows for the direct comparison of the two controllers. In the comparison of those controllers, the signal noise floor is kept constant while the controller penalty is manipulated to reach the desired actuator effort level.

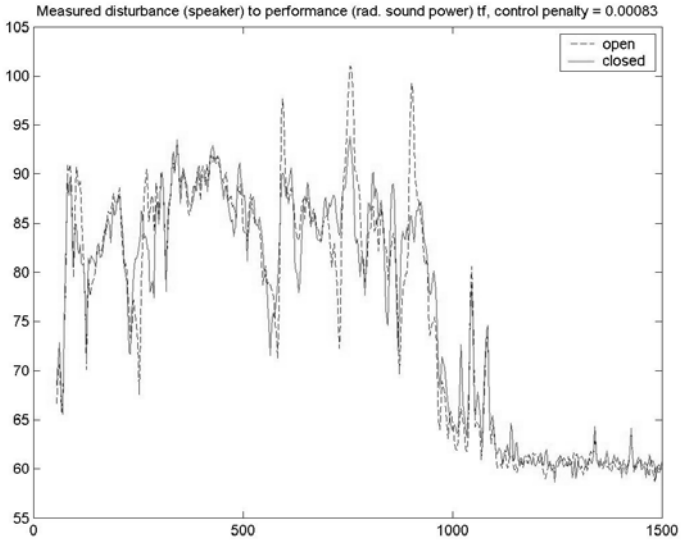

Figure 4: Radiated Sound Power, 0.010 in. Shims, 0.76 Actuator Effort Level

The first group of tests involved the quasi-simply supported case. Nine controllers with varying actuator effort levels were created, and one will be examined here. Creating nine controllers was a way to ensure that similar effort levels would be reproducible for other boundary conditions, providing the data necessary for direct comparison through the variations in the shims. The most aggressive controller that would remain stable for additional tests at other boundary conditions had an actuator effort level of approximately 0.76 and signal noise floor of 30 dB. The results of that controller can be seen in the above figure showing the radiated sound power as a result of the disturbance from the speaker. If radiated sound power reduction is considered across the bandwidth of the plot, the total reduction is only 2 dB.

It can be more beneficial to examine the reduction at specific frequencies. Since the optimization routine involved locating the actuator/sensor pairing to best control the most efficient structural radiation modes, observing the reduction in radiated sound power at those frequencies is key. The following table shows the results of this examination.

Plate Mode	Frequency	Approx. Reduction
(1,1)	107 Hz.	~8 dB
(1,3)	270 Hz.	~6-10 dB
(1,5)	595 Hz.	~8 dB
(3,1)	757 Hz.	~7-8 dB
(3,3)	904 Hz.	~13 dB

Table 2: Approximate Radiated Sound Power Reduction at Target Frequencies, 0.010 in. Shims, 0.76 Actuator Effort Level

It is clear that the reduction in radiated sound power at the specifically targeted modes is much greater than the overall reduction in the bandwidth of the figure. The penalty for this high level of control can also be seen in Figure 4 in the form of spillover (closed loop radiated sound power being higher than the open loop sound power) at certain frequencies. The spillover is not a major concern due to the fact that the increase in radiated sound power at those frequencies does not exceed the level of radiated sound in the overall frequency range. Additional controllers with lower overall actuator effort levels reduce the amount of spillover while at the same time also reducing the amount of approximate reduction modes of interest. The overall sound power reduction for those controllers taken over the bandwidth of interest is still in the 2-3 dB range. Therefore, if a decision needed to be made between several controllers, and actuator effort level was of no consequence, the decision would likely rely on the distinction between radiated sound power reductions at specific frequencies versus reduced overall spillover.

The thickest single shims available for testing were 0.125 in. The same controller design process was followed as in the case of the quasi-simply supported condition. A comparison will be made here between the controllers with the actuator effort level of 0.76.

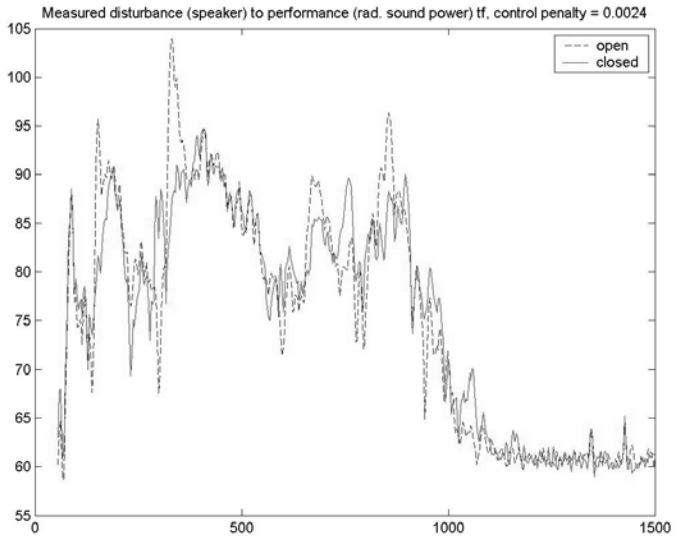

Figure 5: Radiated Sound Power, 0.125 in. Shims, 0.76 Actuator Effort Level

The overall radiated sound power reduction is slightly higher than 3 dB, which is more than in the case of the 0.010 in. shims. The true power of the controller is again seen at the frequencies representing the efficient radiation modes of the plate. The following table examines those frequencies and the approximate reduction in radiated sound power found there.

Plate Mode	Frequency	Approx. Reduction
(1,1)	153 Hz.	~14 dB
(1,3)	332 Hz.	~16 dB
(1,5)	680 Hz.	~5 dB
(3,1)	857 Hz.	~8 dB

Table 3: Approximate Radiated Sound Power Reduction at Target Frequencies, 0.125 in. Shims, 0.76 Actuator Effort Level

For the case of the 0.125 in. shims, the (3,3) mode is beyond 1000 Hz, and is therefore filtered out by hardware filters within the system. The higher reduction in radiated sound power at the specific frequencies is again achieved at the cost of spillover. The spillover is acceptable since it does not exceed the response in the bandwidth of interest.

11. CONCLUSIONS

The work presented in this paper represents an attempt to combine the modeling of structural variations in boundary conditions with an optimization process designed to compensate for those potential variations. The first step in the process required the detailed modeling of a simply supported plate structure with theoretically variable, rotational springs present at the boundaries. Next, detailed models of transducers were created. These models were designed in an efficient way that allowed for simple calculations regarding the spatial coupling of the transducers and the plate. Using these modeled transducers, a genetic algorithm was instituted to attempt convergence on optimal placement locations. The optimal nature of the results was defined by a high level of coupling to important, structural radiating modes within a specific bandwidth of interest, as well as a low level of coupling to out of bandwidth modes. Radiation filters were modeled in order to estimate the radiated sound power from the output of modeled accelerometers.

Once optimal solutions were obtained, a test structure was manufactured that was able to closely replicate the variable boundaries found in the modeled plate. A final optimal location for an actuator/sensor pair was selected based on the results of the genetic algorithm and the efficiency of a controller based on the pairing. Following the collection of data and the identification of the structural system, LQG feedback controllers were designed and implemented in closed loop feedback control with the goal being the minimization of the radiated sound power due to acoustic loading. Tests were conducted at various boundary conditions that were created using a shim mounting technique capable of producing different effective rotational stiffness values based on the thickness of the shims.

For a situation where there are potential variations in the boundary conditions of a plate structure, it is clearly evident that optimizing the placement of an actuator/sensor pair with regards to these potential variations is beneficial. Spatially locating the transducer pair in order to optimally control the efficient structural radiation modes can be extended to achieve control over a boundary condition range.

12. REFERENCES

[1] Fuller, C.R., Hansen, C.H., and Snyder, S.D., 1989. "Active Control of Structurally Radiated Noise Using Piezoceramic Actuators," *Inter-Noise 89*, pp. 509-511.

[2] Fuller, C.R., and Jones, J.D., 1987, "Experiments on reduction of propeller induced interior noise by active control of cylinder vibration," *Journal of Sound and Vibration*, **112**(2), pp. 389-395.

[3] Fuller, C.R., 1990. "Active Control of Sound Transmission/Radiation from Elastic Plates by Vibration Inputs: I Analysis," *Journal of Sound and Vibration*, **136**(1), pp. 1-3.

[4] Grewal, A., Nitzsche, F., Zimcik, D.G., and Leigh, B. "Active Control of Aircraft Cabin Noise Using Smart Structures," *In: AIAA/ASME/AHS Adaptive Structures Forum, Salt Lake City, UT, Apr 18-19, Technical Papers*, 91-100, 1996. *A96-27071 06-39.*

[5] Mathur, G.P., Tran, B.N., Simpson, M.A., and Peterson, D.K. "Broadband Active Structural Acoustic Control of Aircraft Cabin Noise – Laboratory Tests," *American Institute of Aeronautics and Astronautics***,** 1997, 422-431. *AIAA-97-1636-CP.*

[6] Clark, R. L., and Frampton, K. D., "Aeroelastic Structural Acoustic Coupling: Implications on the Control of Turbulent Boundary Layer Noise Transmission," Journal of the Acoustical Society of America, Vol. 102, No. 3, pp. 1639-1647, Sept. 1997.

[7] Frampton, K. D., and Clark, R. L., "Control of Sound Transmission through a Convected Fluid Loaded Plate with Piezoelectric Sensoriactuators," Journal of Intelligent Materials Systems and Structures, Vol. 8, No. 8, pp. 686-696, August 1997.

[8] Frampton, K. D., and Clark, R. L., "Sound Transmission Through an Aeroelastic Plate into a Cavity," AIAA Journal, Vol. 35, No. 7, pp. 1113-1118, July 1997.

[9] Vipperman, J.S. and Clark, R.L., 1996. "Implementation of an Adaptive Piezoelectric Sensoriactuator," *AIAA Journal*, **34**(10), 2102-2109.

[10] Hagood, N.W., Chung, W.H., and Von Flotow, A. "Modeling of Piezoelectric Actuator Dynamics for Active Structural Control". In proceedings of the 31st AIAA/ASMO/ASCA/AHS Structures, Structural Dynamics, and Materials Conference, pages 2242-2256, April 2-4, 1990. *AIAA-90-1087-CP.*

[11] Clark, R.L., Saunders, W.R., and Gibbs, G.P. Adaptive Structures, Dynamics and Control, John Wiley and Sons, NY, 1998.

[12] Elliott, S.J., and Johnson, M.E., 1993. "Radiation Modes and the Active Control of Sound Power," *Journal of the Acoustical Society of America*, **94**(4), 2194-2204.

[13] Gibbs, G.P., Clark, R.L., Cox, D. E., and Vipperman, J.S., 1999. "Radiation Modal Expansion: Application to Active Structural Acoustic Control," *Journal of the Acoustical Society of America*, **107**(1), 332-339.

[14] Clark, R.L., and Cox, D.E., 1999. "Band-Limited Actuator and Sensor Selection for Disturbance Rejection," *AIAA Journal of Guidance, Control, and Dynamics*, **22**(5), 740-743.

[15] Smith, G.C., and Clark, R.L., 1999. "Adaptive Structure Design Through Optimum Spatial Compensation," *Proceedings of Active 99*, Fort Lauderdale, FL, December 2-4.

[16] Richard, R.E., and Clark, R.L., 2000. "Genetic Spatial Optimization of Active Elements on an Aeroelastic Delta Wing," *Proceedings of the ASME Winter Annual Meeting*, Orlando, FL, November 5-10.

[17] Lim, K.B., 1997. "Disturbance Rejection Approach to Actuator and Sensor Placement," *AIAA Journal of Guidance, Control, and Dynamics*, **20**(1), 202-204.

[18] Lim, K.B., and Gawronski, W., 1996. "Hankel Singular Values of Flexible Structures in Discrete Time," *AIAA Journal of Guidance, Control, and Dynamics*, **19**(6), 1370-1377.

[19] Gawronski, W., and Lim, K.B., 1996. "Balanced Actuator and Sensor Placement for Flexible Structures," *International Journal of Control*, **65**(1), 131-145.

[20] Clark, R.L. "Advanced Sensing Techniques for Active Structural Acoustic Control." PhD thesis, Virginia Polytechnic Institute and State University, 1992.

[21] Richard, Robert E. "Optimized Flutter Control for an Aeroelastic Delta Wing." PhD thesis, Duke University, 2002.

[22] Richard, R.E., Rule, J.A., and Clark, R.L., 2001, "Genetic Spatial Optimization of Active Elements on an Aeroelastic Delta Wing," *ASME Journal of Vibration and Acoustics*, **123**(4), 466-471.

[23] Leissa, A., Vibration of Plates, The Acoustical Society of America (reprinting), 1993.